A Dual-Bladder Buoyancy Engine for a Cephalopod-Inspired AUV

Nick Sholl[1,2] and Kamran Mohseni[1,2,3]

***Abstract*— This paper presents a nonlinear, backstepping depth and pitch controller for a dual-bladder buoyancy engine actuated by gear pumps. Flow-rate feedback is obtained using a custom flow sensor comprised of a differential pressure sensor and a small, 3D-printed attachment. The controller is simulated using a model of the CephaloBot, our in-house developed autonomous underwater vehicle (AUV). Its depth control capability is also experimentally validated using a single-bladder buoyancy engine on-board a smaller-scale test cylinder. Lyapunov stability analysis shows global, asymptotic stability, which is exhibited in our simulation. Our experiments verify that this buoyancy engine is a feasible and effective depth controller for AUVs.**

I. Introduction

Autonomous underwater vehicles (AUVs) and remotely operated vehicles (ROVs) are commonly used for ocean exploration and research [1]. Their missions often require that they are able to change and maintain their position in the water column, making it necessary to include an active buoyancy engine on the vehicle. Such buoyancy engines have taken many forms including vertical thrusters [2], external bladders [3], [4], internal ballast tanks [5], [6], and internal bladders, as proposed in this paper.

Vertical thrusters simply push a vehicle up or down in the water column. These thrusters are arguably the most straightforward option for depth control since they generate a control force that is proportional to an applied voltage (unlike bladder or tank based options). They are also less limited in actuation bandwidth than their tank and bladder counterparts. While vertical thrusters may be a good fit for surface-powered ROVs and short-duration AUV missions, their power requirements may be too taxing on an AUV's batteries for longer missions of hours to days, leading to a search for more energy-efficient methods of depth control [7]. Internal or external tanks and bladders, on the other hand, are lower-power solutions for longer missions because they are capable of maintaining a control force without any additional power consumption by directly adjusting the effect of buoyant forces on the vehicle.

Tanks and bladders adjust a vehicle's buoyancy either by changing its volume or its mass. Displacing water outside the main body of the vehicle serves to change the buoyant force acting on it. External bladders typically adjust volume by transferring a fluid, whether it be a gas (air) [5] or liquid (generally oil) [3], [4], from an internal container. Internal tanks and bladders adjust the mass of the vehicle by changing the amount of water inside it, either increasing or decreasing gravitational forces on the vehicle. The fluid transfer in both external and internal tanks can be accomplished using single-stroke pistons [3], [4], which are limited in actuation bandwidth, pumps [6], [8], [9], which are limited by battery power, or compressed gas supplies [5], which are limited by the volume of gas stored on-board. Both of these types of buoyancy adjustment, however, are able to create constant depth control forces on the vehicle by shutting off their respective actuators and maintaining a constant volume of fluid in their tanks or bladders.

The downside of tanks and bladders is that their dynamics inherently require more complicated control strategies than those of thrusters to achieve a reasonable transient performance. This is due to the fact that increasing the control input, which usually results in increased flow rate into a bladder or tank, does not directly exert a force on the vehicle. Instead, it changes the derivative of the buoyant force on the vehicle [9].

Many buoyancy engines, regardless of their actuation strategy, are able to generate pitch moments [7], [9]–[11] in addition to controlling depth. While many AUVs are designed so that they are inherently roll stable, such as our group's CephaloBot [12] and DAUV [13] platforms, they can still benefit from the ability to control pitch to, for example, point a camera or a light. Some vehicles even use pitch and buoyancy adjustments to propel themselves in the global x-y plane, in addition to the global z frame. These underwater gliders are generally intended for long-duration missions and have unique propulsion systems to accommodate those missions. For example, the Slocum Thermal utilizes thermal reactions to adjust its density [14]. When it passes a thermocline (a water-temperature boundary in a body of water), a material inside it melts or freezes, changing in volume as it does so. This adjusts the vehicle's buoyancy and pitch such that wings at the aft of the vehicle provide forward propulsion as a result of motion in the global z direction.

This paper presents experimental results of single-bladder depth control and simulated results of dual-bladder depth and pitch control. A nonlinear backstepping control technique is

[1] Department of Mechanical and Aerospace Engineering, University of Florida, Gainesville, FL

[2] Institute for Networked Autonomous Systems, University of Florida, Gainesville, FL

[3] Department of Electrical and Computer Engineering, University of Florida, Gainesville, FL

used to control the buoyancy engine in both cases. Section II describes the testing platforms, section III describes the control strategy, and section IV presents our experimental and simulated results. These results are discussed in section V, and future work is outlined in section VI.

II. Buoyancy Engine and Vehicle Design

Here, we describe the design of our buoyancy engine and the two vehicles it is installed on.

A. Buoyancy Engine

The buoyancy engines on our vehicles described below are comprised of either one or two buoyancy modules. Each module adjusts the density of the vehicle by pumping water in and out of the CephaloBot. A diagram of the component layout is shown in Fig. 1. Each buoyancy module consists of a valve (GEMS Sensors & Controls A2017-C203), a gear pump (Greylor PQ-12DC), and a custom buoyancy bladder which holds 0.36 kg when full. A 3D-printed (3D Systems Projet 2500 Plus) attachment for a 25 kPa differential pressure sensor (Freescale Semiconductor MPXV7025DP) provides flow rate feedback for the gear pump. An absolute pressure sensor (Freescale Semiconductor MPXHZ6250A) monitors the bag pressure to prevent the pump from applying high or low enough pressures to break the seals on the bag, potentially flooding the vehicle.

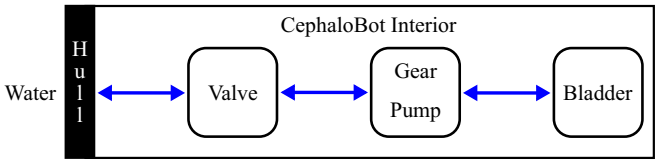

Fig. 1: CephaloBot buoyancy engine diagram. The engine pumps water from the environment into and out of the vehicle to adjust the vehicle's density.

B. CephaloBot

The buoyancy engine and controller presented in this paper are designed for our group's AUV, the CephaloBot [12] (Fig. 2). This system consists of two of the buoyancy modules (Fig. 3) described in section II-A. By placing the modules in the fore and aft of the AUV, the changes in mass of the bladders can be exploited to create a pitch moment on the vehicle in addition to adjusting the vehicle's density for depth control. A model of the system is used in this paper to simulate the effectiveness of the proposed controller and buoyancy engine.

C. Buoyancy Test Cylinder

Before implementing multiple buoyancy modules on the CephaloBot AUV, a test cylinder (Fig. 4) was constructed to validate the efficacy of the buoyancy engine design for 1-degree-of-freedom (DOF) depth control. The test cylinder is controlled by an Arduino Mega which handles all sensor measurements and control algorithm calculations. Power and surface communications are transmitted through a tether

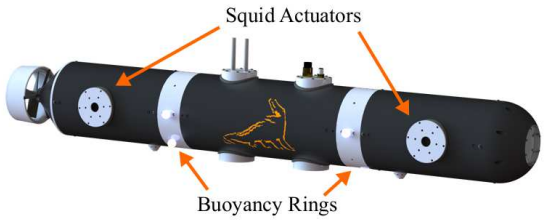

Fig. 2: Render of the CephaloBot AUV with new buoyancy engine ring modules. Each ring houses a buoyancy bladder, valve, and pump. Like the squid actuators on the vehicle, the buoyancy engine incorporates compliant components in its design.

Fig. 3: CephaloBot buoyancy ring shown with pump, valve, and bladder. Pressure sensors (not shown) used to monitor bladder pressure and pump flow rate are installed in-line between the pump outlet and the bladder inlet.

via a wetmate connector. This system includes a single module buoyancy engine, as described in section II-A, with a maximum bladder capacity of 0.36 kg. The test cylinder has a mass of 6.97 kg with an empty bladder. Depth is measured with a 15 psi gage pressure sensor (Honeywell FP2000) capable of providing sub-millimeter depth resolution.

III. Buoyancy Control

A nonlinear control strategy has been employed to control the proposed buoyancy engine. In this section, we outline the dynamics of the CephaloBot AUV, describe our assumptions, and formulate our controller.

A. CephaloBot Dynamics

The standard dynamic equations for underwater vehicles are

$$\dot{\eta} = J\nu, \tag{1}$$

$$M\dot{\nu} + (C(\nu) + D(\nu))\nu + g(\eta) = \tau, \tag{2}$$

where M is the inertia matrix, $C(\nu)$ is the Coriolis matrix, $D(\nu)$ is the drag matrix, $g(\eta)$ is the vector of restoring

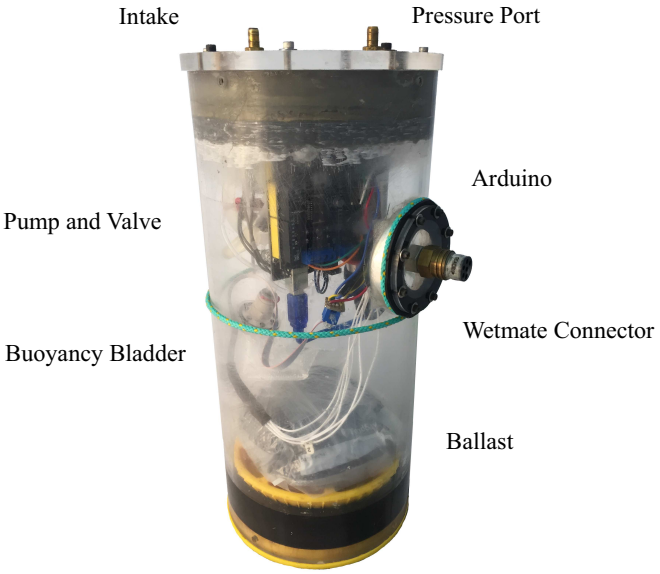

Fig. 4: Buoyancy test cylinder with a single-bladder buoyancy engine. A pump controls the amount of water in an internal buoyancy bladder using an in-line flow sensor for feedback. Pump commands, depth calculations via pressure measurement, and control algorithm calculations are handled by an on-board Arduino Mega. Power and surface communications are transmitted through a tether via the wetmate connector. Lead ballast ensures that the system is neutrally buoyant when the bladder is at half capacity. The mass of the system with an empty buoyancy bladder is 6.97 kg, and the buoyancy bladder has a maximum capacity of 0.36 kg.

forces (not including forces from the buoyancy engine), and τ is the vector of control forces from the buoyancy engine with respect to the body frame [15]. The vector $\eta = \begin{bmatrix} x & y & z & \phi & \theta & \psi \end{bmatrix}^T$ is the position vector in the global frame, and η_d is the desired position vector. For this paper, the heading (yaw) ψ, roll ϕ, and x and y positions are considered constant and zero. A tensor $J(\eta)$ rotates the global coordinates to the body frame, yielding the body velocity vector $\nu = \begin{bmatrix} u & v & w & p & q & r \end{bmatrix}^T$, where v, p, and r are zero as a result of the restrictions placed on η.

The vector of control forces is defined as

$$\tau = {}^{Body}\tau = J^{-1}\ {}^{Global}\tau,$$

where

$${}^{Global}\tau = \begin{bmatrix} F_x & F_y & F_z & M_\phi & M_\theta & M_\psi \end{bmatrix}^T.$$

The only components considered for this controller (Fig. 5) are the forces in the direction of gravity (F_z) and the pitch moment (M_θ). All other forces in the global frame are set to zero. Note that because the forces all rely on gravity, τ becomes a function of η.

Balancing the force due to the mass of the vehicle, the forces generated by the buoyancy engine, and the buoyant force on the vehicle in the global z direction yields

$$F_z = M_{vehicle}g + F_{B1} + F_{B2} - \rho V_{Vehicle}g, \tag{3}$$

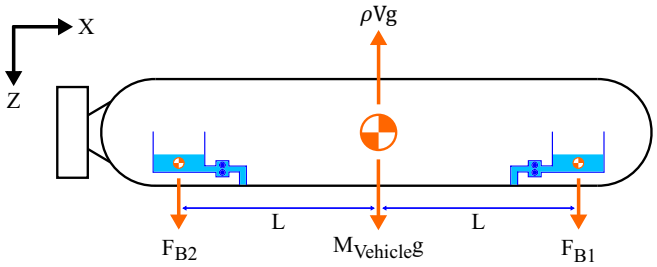

Fig. 5: Free body diagram of the CephaloBot AUV for 2D pitch and depth control. Fore and aft buoyancy control units are individually controlled to adjust both the depth and pitch of the vehicle.

where $M_{vehicle}$ is the mass of the vehicle, $V_{Vehicle}$ is the total volume of the AUV, and the forces from each buoyancy module are defined as

$$\begin{aligned} F_{B1} &= m_{B1}g, \\ F_{B2} &= m_{B2}g, \end{aligned} \tag{4}$$

where m_{B1} and m_{B2} are the masses of buoyancy module 1 and 2, respectively. Since control of the buoyancy engine takes effect at the flow rate level as opposed to the mass level, the derivative of F_z must be taken, giving

$$\dot{F}_z = \dot{F}_{B1} + \dot{F}_{B2} = \rho g(u_1 + u_2), \tag{5}$$

where u_1 and u_2 are the volume flow rates in buoyancy engines 1 and 2, respectively.

The pitch moment on the vehicle is defined as

$$M_\theta = L\cos\theta(F_{B2} - F_{B1}) \tag{6}$$

where L is the distance of each buoyancy module to the center of mass of the vehicle and θ is the pitch of the vehicle included in η. The derivative of M_θ must also be taken to relate it to the control signal:

$$\dot{M}_\theta = \rho g L\cos\theta(u_2 - u_1) - \sin\theta\dot{\theta}(F_{B2} - F_{B1}). \tag{7}$$

This gives us

$${}^{Global}\dot{\tau} = \begin{bmatrix} 0 & 0 & \dot{F}_z & 0 & \dot{M}_\theta & 0 \end{bmatrix}^T, \tag{8}$$

which can be used to solve for the desired flow rates.

B. Assumptions

The following assumptions were made about the dynamics presented in section III-A to facilitate the formulation of this buoyancy engine controller:

1) Since the vehicle is fairly well modeled, the hydrodynamic constants M, C, D and g are assumed to be known.
2) Values of η and ν are assumed measurable since our testing facility is equipped with a Qualisys underwater motion-capture system.
3) $D(\nu)$ can be treated as a constant in the desired operating range.
4) The AUV is neutrally buoyant when the buoyancy bladders are at half capacity to ensure maximum control authority in both directions.
5) The AUV is constrained in all DOF except for depth and pitch, simplifying the problem to 2 DOF.

6) The masses of each buoyancy module can be considered measurable by taking the integral of the measured flow rate.

C. Controller Formulation

Here we describe our nonlinear backstepping controller formulation. The controller is designed to regulate the depth and pitch of the vehicle using the proposed buoyancy engine. To do this, a position error term e which will be driven to zero is defined as

$$e = \eta - \eta_d, \tag{9}$$

where $\eta_d, \dot{\eta}_d, \ddot{\eta}_d$, and $\dddot{\eta}_d$ are known, bounded, continuous functions. Relating the control input u to our error signal e in (9) requires three integrators. We employ a backstepping technique with three backsteps to handle these three integrators in our controller [16]. The first backstep relates the error signal to the vehicle velocity, the second backstep relates the velocity to the acceleration, and the third backstep relates the acceleration to the buoyancy engines' flow rate control inputs.

The derivative of the error is

$$\dot{e} = J\nu - \dot{\eta}_d. \tag{10}$$

We insert a virtual desired velocity controller ν_d into (10) and define a backstepping error η_1 to give us

$$\dot{e} = J\eta_1 + J\nu_d - \dot{\eta}_d, \tag{11}$$

where η_1 is defined as

$$\eta_1 = \nu - \nu_d \tag{12}$$

and ν_d is chosen to be

$$\nu_d = J^{-1}(\dot{\eta}_d - K_1 e), \tag{13}$$

leaving us with

$$\dot{e} = J\eta_1 - K_1 e. \tag{14}$$

Taking the derivative of the first backstepping error, premultiplying by M, and defining a second virtual controller τ_d yields

$$M\dot{\eta}_1 = -\left(C(\nu) + D(\nu)\right)\nu - g(\eta) + \eta_2 + \tau_d - M\dot{\nu}_d, \tag{15}$$

where the second backstepping error η_2 is defined as

$$\eta_2 = \tau - \tau_d \tag{16}$$

and the derivative of the desired velocity vector is

$$\dot{\nu}_d = \dot{J}^{-1}(\dot{\eta}_d - K_1 e) + J^{-1}(\ddot{\eta}_d - K_1 \dot{e}). \tag{17}$$

Choosing the desired vector of control forces τ_d to be

$$\tau_d = \left(C(\nu) + D(\nu)\right)\nu + g(\eta) + M\dot{\nu}_d - Je - K_2\eta_1, \tag{18}$$

we are left with

$$M\dot{\eta}_1 = \eta_2 - Je - K_2\eta_1. \tag{19}$$

Finally, performing a third backstep,

$$\dot{\eta}_2 = J^{-1}\dot{\tau} + \dot{J}^{-1}\tau - x, \tag{20}$$

where

$$\begin{aligned} x = {} & \left(C(\nu) + D(\nu)\right)\dot{\nu} + g(\dot{\eta}) \\ & - K_2\eta_1 + M\ddot{\nu}_d - \dot{J}e - J\dot{e}, \end{aligned} \tag{21}$$

the second derivative of the desired velocity is

$$\begin{aligned} \ddot{\nu}_d = {} & \ddot{J}^{-1}(\dot{\eta}_d - K_1 e) + 2\,\dot{J}^{-1}(\ddot{\eta}_d - K_1\dot{e}) \\ & + J^{-1}(\dddot{\eta}_d - K_1\ddot{e}), \end{aligned} \tag{22}$$

and

$$\ddot{e} = \ddot{J}\nu + J\ddot{\nu} - \dddot{\eta}_d. \tag{23}$$

Choosing the controller to be

$$u = J(x - \eta_1 - K_3\eta_2 - \dot{J}^{-1}\tau) \tag{24}$$

leaves us with

$$\dot{\eta}_2 = -\eta_1 - K_3\eta_2. \tag{25}$$

D. Lyapunov Stability Analysis

A Lyapunov candidate for the above system is chosen as

$$V = \frac{1}{2}e^T e + \frac{1}{2}\eta_1^T M\eta_1 + \frac{1}{2}\eta_2^T\eta_2. \tag{26}$$

Taking the derivative of the Lyapunov candidate yields

$$\begin{aligned} \dot{V} &= e^T\dot{e} + \eta_1^T M\dot{\eta}_1 + \eta_2^T\dot{\eta}_2 \\ &= -K_1 e^T e - K_2\eta_1^T\eta_1 - K_3\eta_2^T\eta_2, \end{aligned} \tag{27}$$

which is negative definite, proving that the system is asymptotically stable. By defining z as

$$z = \begin{bmatrix} e^T & \eta_1^T & \eta_2^T \end{bmatrix}^T \dot{V} = -2KV, \tag{28}$$

it is possible to show that, for $K = \min(K_1, K_2/M, K_3)$, the states are bounded by

$$\|z(t)\| \leq \|z(0)\|\,\mathrm{e}^{-\mathrm{Kt}}, \tag{29}$$

suggesting that the controller will be exponentially stable. Given our current hardware, however, actuator saturation prevents the system from achieving this exponential stability.

IV. Results

We tested the proposed controller in a simulation of our CephaloBot AUV and experimentally with our test cylinder. Here, we present the data from these tests.

A. CephaloBot Simulation

Applying the controller presented in section III to our existing model of the CephaloBot shows that the AUV should be capable of converging asymptotically to a depth of 1.6 m and a 0 degree pitch with a step input (Fig. 6). While the buoyancy bladders saturate for a short period of time, the maneuver uses implementable control signals and does not exceed the actual actuation authority of the buoyancy engine. The simulated vehicle reaches a top dive speed of 15.8 cm/s. When the hydrodynamic coefficients are adjusted such that the controller expects 20% higher values than the actual coefficients, the controller increases the top dive speed to 17.2 cm/s but remains stable with no overshoot.

B. Test Cylinder Experiment

Pool trials of the buoyancy test cylinder provided the results shown in Fig. 7. The trial shown overshoots the depth set point by 42 cm before settling to a window of $\pm$8.5 cm. The mass estimate overshoots the actual bladder maximum mass by 50 g before settling to within $\pm$18.2 g of the neutral buoyancy bag mass. Taking the derivative of the depth signal and applying a moving average filter over 30 data points (0.6 s) suggests a maximum dive speed of 42 cm/s.

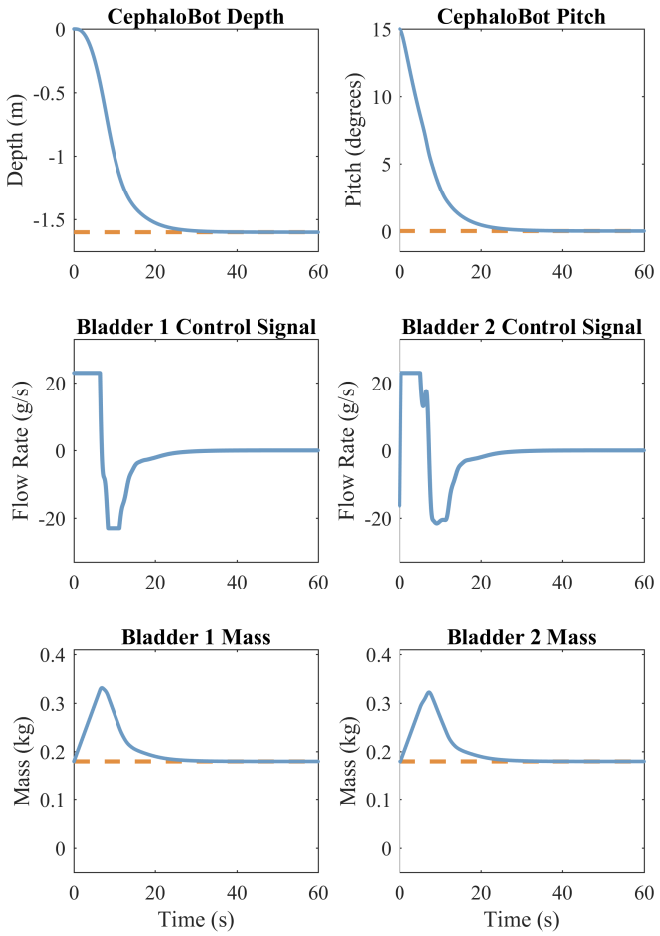

Fig. 6: Simulated CephaloBot depth and pitch controller performance. Dashed lines show the depth set point, the pitch set point, and the neutral buoyancy points for both bladders.

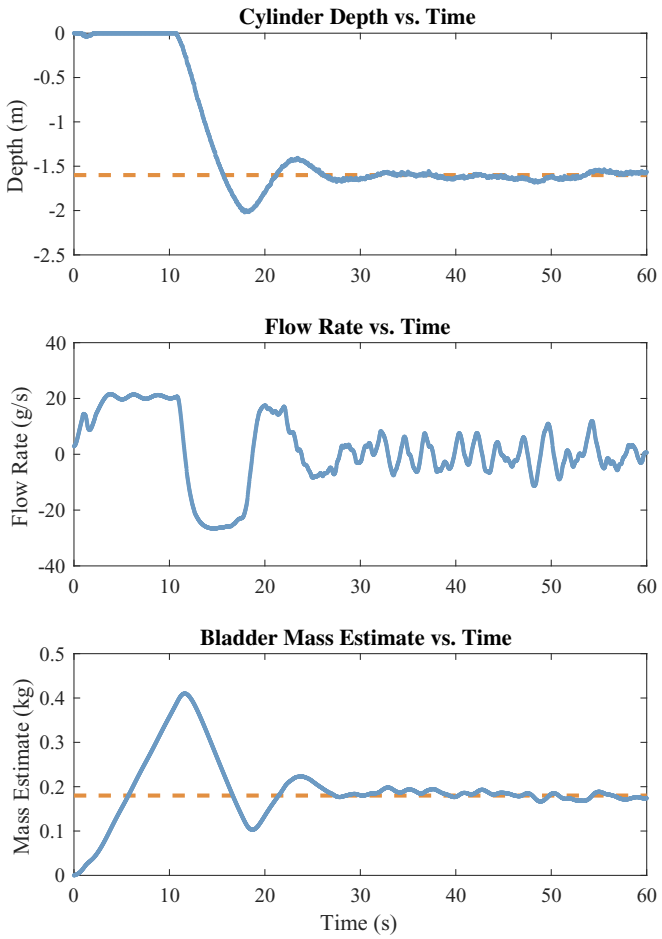

Fig. 7: Experimental results of test cylinder trials in an indoor water tank. Dashed lines show the depth set point and bladder neutral buoyancy point.

V. Discussion

As expected, the CephaloBot simulation shows much better performance than the test cylinder pool trials, and there are several likely explanations for this discrepancy. The most likely cause is the assumption in the control formulation that the hydrodynamic coefficients of the system are known. If this assumption is removed, only a globally, uniformly bounded result can be obtained, as opposed to the asymptotic convergence expected from the presented controller. Evidence of this behavior is shown in the experimental results, which we predicted since the test cylinder's hydrodynamic coefficients have not been as well tested as the CephaloBot's. Pool testing performance was likely also degraded by unmodeled disturbances in the test tank, including but not limited to small thermally induced currents in the tank and forces or drag from the tether providing power and communications. Although efforts were made to reduce these effects, they likely still influence the system's performance.

Designing this buoyancy engine with a gear pump instead of a piston pump allows us to take advantage of higher flow rates in and out of the bladder, but it also removes the reliable flow rate feedback that an encoder can provide on a piston pump. We have observed an issue with measuring low flow rates due to hysteresis in the differential pressure sensor used. This issue could explain some of the noisy response past 30 seconds in the trial shown in Fig. 7. It could also explain the over-estimation of the bladder mass in the experiment.

While the simulation predicts that the vehicle will not overshoot the depth set point, pool testing exhibited a substantial overshoot. It is possible to tune the gains such that there is no overshoot, but in this case where the hydrodynamic coefficients are poorly modeled, the trade-off for reducing overshoot is increasing the steady-state error band. For these tests, the design choice was made to tune the test cylinder to be underdamped, but damping will be increased on the CephaloBot to avoid damaging the vehicle by hitting the bottom of the test tank.

The maximum functional depth of this bladder-based design is limited by the pressure differential that can be generated by the chosen gear pump. Because the CephaloBot and test cylinder do not contain mechanisms to equalize the pressure between their interiors and the surrounding water,

the gear pump must fight that pressure differential when running. If the vehicles dive too deep, the gear pump may fail to resist the external pressure differential, potentially resulting in bladder failure or an inability to empty the bag to surface.

Despite the above issues, the buoyancy engine and controller presented show promise. Unlike many other buoyancy bladder controllers, this controller does not rely on gain scheduling techniques. This avoids potential issues with switching dynamics and reduces the difficulty of tuning by limiting the number of gains that must be tuned. It also differs from other bladder-based buoyancy engines in its high actuation rates. The higher gear pump flow rate allows this controller to respond to disturbances faster than piston-based counterparts. Finally, PID control of the gear pump, as opposed to on-off control, allows variable flow-rate control signals to be used, making the controller continuous.

This controller's utility is not limited to the CephaloBot. With minor modifications to the controller or platform, the proposed controller could also be employed for dynamic, continuous, coupled depth and pitch control on the Seahorse AUV [9], the variable buoyancy system described in [10], or any other dual-bladder/tank systems.

VI. Conclusions

This paper experimentally validates a new buoyancy engine design for the CephaloBot AUV. A nonlinear, backstepping controller for depth and pitch regulation was formulated, implemented in a 1-DOF depth regulation case, and simulated in a 2-DOF depth and pitch regulation case. Lyapunov stability analysis proves that the system is asymptotically stable for the given assumptions, and the simulation verifies this assertion.

Future work will entail full implementation of this design on the CephaloBot. This includes improvements on the flow-rate feedback system. By implementing a Kalman filter with pressure and IMU data, it should be possible to reduce the flow-rate estimation error, thereby decreasing the steady state error. An adaptive element will also be added to the controller to reduce errors in the hydrodynamic vehicle model.

Acknowledgments

We would like to thank the Office of Naval Research and the National Science Foundation for supporting this research. The first author was funded by the Department of Defense (DoD) through the National Defense Science & Engineering Graduate Fellowship (NDSEG) Program. Special thanks to Robyn Natherson for her assistance with test cylinder fabrication and flow sensor characterization.

Author Disclosure Statement

No competing financial interests exist.

References

[1] R. Capocci, G. Dooly, and Omerdić, "Inspection-class remotely operated vehicles a review," *Journal of Marine Science and Engineering*, vol. 5, no. 1, p. 13, 2017. [Online]. Available: http://www.mdpi.com/2077-1312/5/1/13

[2] N. Fischer, D. Hughes, P. Walters, E. M. Schwartz, and W. E. Dixon, "Nonlinear rise-based control of an autonomous underwater vehicle," *IEEE Transactions on Robotics*, vol. 30, no. 4, pp. 845–852, 2014.

[3] E. J. Berkenpas, B. S. Henning, C. M. Shepard, A. J. Turchik, C. J. Robinson, E. J. Portner, D. H. Li, P. C. Daniel, and W. F. Gilly, "A buoyancy-controlled lagrangian camera platform for in situ imaging of marine organisms in midwater scattering layers," *IEEE Journal of Oceanic Engineering*, vol. 43, no. 3, pp. 595–607, 2018.

[4] E. A. D'Asaro, "Performance of autonomous lagrangian floats," *Journal of Atmospheric and Oceanic Technology*, vol. 20, no. 6, pp. 896–911, 2003.

[5] T. Love, D. Toal, and C. Flanagan, "Buoyancy control for an autonomous underwater vehicle," *Guidance and Control of Underwater Vehicles 2003*, vol. 36, no. 4, pp. 199–204, 2003. [Online]. Available: http://dx.doi.org/10.1016/S1474-6670(17)36681-8

[6] W. J. Kirkwood and D. E. Steele, "Active variable buoyancy control system for mbari's rov," *Proceedings of OCEANS'94*, vol. 2, pp. II/471–II/476, 1994.

[7] C. Detweiler, S. Sosnowski, I. Vasilescu, and D. Rus, "Saving energy with buoyancy and balance control for underwater robots with dynamic payloads," *Springer Tracts in Advanced Robotics*, vol. 54, pp. 429–438, 2009.

[8] L. Reste, "Deep-Arvor: A new profiling float to extend the argo observations down to 4000-m depth," *Journal of Atmospheric and Oceanic Technology*, vol. 33, no. 5, pp. 1039–1055, 2016.

[9] S. Tangirala and J. Dzielski, "A variable buoyancy control system for a large auv," *IEEE Journal of Oceanic Engineering*, vol. 32, no. 4, pp. 762–771, 2007.

[10] M. MacLeod and M. Bryant, "Dynamic modeling, analysis, and testing of a variable buoyancy system for unmanned multimodal vehicles," *IEEE Journal of Oceanic Engineering*, vol. 42, no. 3, pp. 511–521, 2017.

[11] K. H. Low, "Design, development and locomotion control of bio-fish robot with undulating anal fins," *International Journal of Robotics and Automation*, vol. 22, no. 1, pp. 88–99, 2007.

[12] M. Krieg, P. Klein, R. Hodgkinson, and K. Mohseni, "A hybrid class underwater vehicle: Bioinspired propulsion, embedded system, and acoustic communication and localization system," *Marine Technology Society Journal*, vol. 45, no. 4, pp. 153–164, 2011.

[13] Z. Y. Song, C. Mazzola, E. Schwartz, R. R. Chen, J. Finlaw, M. Krieg, and K. Mohseni, "A compact autonomous underwater vehicle with cephalopod-inspired propulsion," *Marine Technology Society Journal*, vol. 50, no. 5, pp. 88–101, 2016.

[14] R. Davis, C. Eriksen, and C. Jones, "Autonomous buoyancy-driven underwater gliders," *Technology and Applications of Autonomous Underwater Vehicles*, pp. 37–58, 2002. [Online]. Available: http://www.crcnetbase.com/doi/10.1201/9780203522301.ch3

[15] T. I. Fossen, *Marine Control Systems: Guidance, Navigation and Control of Ships, Rigs and Underwater Vehicles*. Trondheim, Norway: Marine Cybernetics, 2002.

[16] H. K. Khalil, *Nonlinear Systems*. Prentice Hall, 2002.